Evidence of the 17-keV neutrino in the β spectrum of ^{3}H

A. Hime* and J. J. Simpson
Department of Physics and Guelph-Waterloo Program for Graduate Work in Physics, University of Guelph, Guelph, Ontario, N1G 2W1, Canada
(Received 9 September 1988)

A measurement of the β spectrum of tritium implanted into a hyperpure germanium detector is reported. A distortion is observed 17 keV below the end point which is in agreement with an earlier measurement involving a tritium-implanted Si(Li) detector. The excess of counts observed in the low-energy region of the tritium spectrum is best described by the emission of a 16.9±0.1 keV neutrino and a mixing probability between 0.6 and 1.6% when allowance is made for uncertainty in the effective screening potential appropriate for tritium bound within a crystal lattice.

I. INTRODUCTION

The β spectrum of tritium, implanted into a Si(Li) x-ray detector, shows a distortion 17 keV below the end point.[1,2] This was interpreted as evidence for the emission of a 17-keV neutrino with a 2–4 % mixing probability. A number of authors[3–6] have pointed out that corrections to the screening potential and exchange effects, in the case of atomic tritium, would reduce the excess of counts observed in the low-energy region of the β spectrum and thus reduce the quoted mixing probability. For example, when the published spectra are analyzed using the effective screening potential suggested by Lindhard and Hansen[5] for free tritium the mixing probability for a 17-keV neutrino is reduced to 1.6%. However, in the extreme case that the effective screening potential is reduced to zero the excess of counts in the low-energy region of the tritium spectrum does not disappear and is still consistent with the emission of a 17-keV neutrino with a 0.5% mixing probability. Consequently, the distortion does not seem to be entirely attributable to atomic-physics effects. (See Appendix C.)

A number of experiments searching for a similar distortion in other β spectra were carried out. Reports[7–11] describing measurements of the β spectrum of ^{35}S have been published, all claiming very low limits for the emission of a 17-keV neutrino (some as low as 0.15%). However, these results have been criticized[2,12] and several have been reinterpreted to suggest that they are consistent with the emission of a 17-keV neutrino. More recently an experiment on ^{63}Ni has been reported[13] claiming a mixing probability $\sin^2\theta \lesssim 0.3\%$ for a 17-keV neutrino.

Although, to date, no other experiment on the tritium β spectrum has been reported which directly refutes the ^{3}H result reported earlier, it was deemed important to attempt to check the earlier result by measuring the ^{3}H β spectrum in a different detector. In the experiment reported here, tritrium was implanted into a hyperpure germanium crystal operating as a source-detector combination similar to the Si(Li) detector system. However, as shall be described below, the germanium-detector measurements have some significant differences and advantages relative to the Si(Li) detector measurement which permit the estimation of systematic effects which were unresolved in the earlier experiment. When it was finally apparent that the data about to be described confirmed the distortion in the ^{3}H spectrum, a ^{35}S experiment was carried out which is reported in the preceding paper.[14]

II. GENERAL CONSIDERATIONS

If there is an advantage in measuring the tritium β spectrum by implanting tritons into a solid-state detector it lies in the simplicity of the method. This approach provides a total absorption spectrometer which automatically eliminates the difficulties that can arise when using sources that are external to the detecting apparatus. While a detailed description of the technique of implanting tritium into a cooled Si(Li) detector has already appeared[15] it is our aim, in this section, to motivate a new experiment where tritium is embedded in a hyperpure germanium detector. In particular, emphasis is on features of the germanium experiment that aid in circumventing some uncertainties associated with the Si(Li) experiment with respect to the 17-keV neutrino hypothesis.

Of primary concern when bombarding a semiconductor with high-energy ions is the potential for inducing radiation damage within the crystal lattice. Studies of proton and α-particle bombardment of Si and Ge crystals have shown that the radiation damage induced is primarily in the form of Frenkel defects.[16] These defects in turn act as trapping centers for electrons and holes produced by ionizing radiation which manifest themselves as pulse-height defects.[17] It is known[18] that radiation damage in germanium can be removed by annealing at temperatures $\lesssim 200\,^\circ$C and that hydrogen is tightly bound in germanium for temperatures up to 500 °C (Ref. 19). Hence it is feasible to implant tritium into pure germanium and achieve annealing temperatures that are sufficient to cure radiation damage without affecting the tritium.

By confining the tritium beam to the central region of the detector possible distortions associated with tritium nuclei decaying near the edges of the crystal can be avoided. In addition, the extent of radiation damage and its effect on the response of the detector can be monitored

by scanning the detector surface across implanted as well as nonimplanted regions of the crystal using a narrow beam of photons. At the same time the tritium can be implanted at a depth sufficient to absorb electromagnetic radiation such as internal or external bremsstrahlung[20] produced within the detector when β particles are emitted. Also, β particles with energies above the K absorption edge of germanium (11.1 keV) can ionize the K shell of Ge atoms and produce Ge x rays. If any of these radiative processes occur near a detector surface the radiation could escape the crystal unnoticed, thus yielding an incorrect measurement of the full β energy. Since the maximum allowed β energy in tritium decay is $\sim$18.6 keV it is sufficient to implant tritium at a depth which is large in comparison to the mean absorption length of 18.6 keV photons in germanium ($\sim$20 μm). In this way difficulties associated with radiation escaping the detector can be circumvented.

Nuclear scattering can lead to tritium atoms stopping near ($\sim$10 μm) to the surface of the detector provided this scattering takes place within the first $\sim$50 μm of the triton path. A rough estimate indicates that $\lesssim 10^{-7}$ tritium atoms as a fraction of the total implanted would be near the surface.

It is convenient to implant tritium while the germanium crystal remains housed in its cryostat. This is possible for spectrometers which have thin windows covering the detector. In this case a thin beryllium window ($\sim$0.08 mm) covers the germanium crystal so that 14-MeV tritons are sufficient for implanting to a depth of $\sim$0.35 mm.

Since the primary interest is in studying the lower-energy portion of the tritium β spectrum (0–5 keV), it is important to be able to calibrate the spectrometer at low energies. In general this is difficult for solid-state detectors due to the low penetrability of x rays with energy below $\sim$5 keV in the materials covering the sensitive volume of the detector and in the dead layer of the detector itself. However, by fluorescing the germanium crystal with photons above the Ge K absorption edge (11.1 keV) the K escape peaks can be used for calibrating the detector at low energies. For example, when Br K_α x rays ($\sim$11.9 keV) are incident on Ge a fraction of the interactions produce Ge K_α x rays (9.9 keV). If such interactions take place near the crystal surface some of the Ge x rays will escape the detector leaving a photopeak at 2 keV. Hence, by fluorescing materials with a range in Z between that of Se and Mo, calibration lines can be produced between $\sim$1.3 keV and 19.7 keV, which cover essentially the entire β-energy range.

III. EXPERIMENT

A. Implantation procedure

The detector in which the tritium is implanted consists of a nominal 200-mm^2-by-7-mm-thick hyperpure germanium crystal housed inside a horizontal cryostat covered with a 0.08-mm-thick beryllium window and cooled to liquid-nitrogen temperature. In order to locate the edges of the detector a scan along the horizontal and vertical axes of the crystal surface was made using the 5.9-keV x rays of ^{55}Mn before implanting. It was found that the active area of the germanium crystal has a diameter of $\sim$15.5 mm and is centrally located within its cryostat to within $\sim$0.5 mm.

A tritium beam was obtained from the FN tandem Van de Graff accelerator at McMaster University. As illustrated in Fig. 1 this beam passed through a 0.013-mm tantalum window at the end of the beam pipe, and into the detector through its beryllium window. A 10-mm-diameter tantalum collimator was mounted so that tritons were implanted away from the edges of the crystal. As a result an $\sim$3-mm annulus of nonimplanted germanium remains which allows for scanning through implanted and nonimplanted regions of the detector with a narrow beam of photons.

For most of the implantation the triton energy ranged from $\sim$13.5 MeV to 14.3 MeV. These energies were sufficient for implanting tritium to depths[21] of $\sim$0.28 mm to 0.32 mm, which is large in comparison to the absorption length of 18.6-keV bremsstrahlung photons ($\sim$20 μm) and thus large relative to the mean path length of 18.6-keV β particles ($\sim$1.6 μm) in germanium. A final

TABLE I. Specific features of tritium implants.

Triton energy (MeV)	Beam current (nA)	Duration of burst (s)	No. of tritons implanted	Mean implant depth (mm)
13.50	0.05	45	1.4×10^{10}	0.280
13.75	0.05	30	0.9×10^{10}	0.295
13.85	0.05	37	1.2×10^{10}	0.300
14.00	0.05	16	0.5×10^{10}	
	0.25	8	1.2×10^{10}	
	0.50	4	1.2×10^{10}	0.305
14.15	0.05	43	1.3×10^{10}	0.315
14.30	0.05	200	6.3×10^{10}	0.320
20.00	0.25	15	2.3×10^{10}	0.590
		Total	1.6×10^{11}	

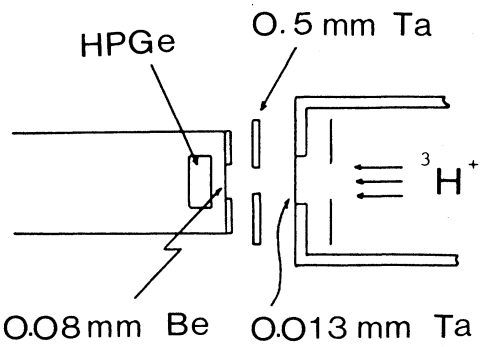

FIG. 1. Illustration of implantation procedure. A tritium beam passed through a tantalum window into the germanium crystal through its beryllium window. A 10-mm tantalum collimator was used to keep tritons away from the edges of the crystal leaving a 3-mm annulus of nonimplanted germanium.

dose of tritium was administered at an energy of ~20 MeV which implanted 13% of the total number of tritons at a depth of ~0.59 mm. Approximately 1.6×10^{11} tritons were implanted in total yielding a net count rate in the neighborhood of 400 cps. Table I lists the parameters characterizing the tritium implantation procedure. At the bombarding energies used, range straggling is about 2% of the mean range.[22]

B. Annealing of radiation damage

The extent of radiation damage induced in the germanium crystal after implanting the tritium was monitored with a narrow beam of 59-keV γ rays from ^{241}Am. The mean absorption length of 59-keV photons in germanium is ~1.0 mm so that this provides a good probe of the detector response at depths including the implanted region. Figure 2 is the result of a scan across the detector diameter directly after implanting tritium. In the first place [Fig. 2(a)] a pulse-height defect of ~2% was observed when photons were incident on that region of the crystal where tritium entered the detector. Second, a reduction in intensity of the photopeak was observed, again in the region where the tritium entered the detector [Fig. 2(b)]. This attenuation in count rate can be attributed to an effective dead layer (~0.59 mm) induced in the detector which extends from the front face of the crystal to a depth corresponding to the end of the highest-energy triton track. Both of these effects will give rise to a distorted β spectrum since incomplete charge collection yields a false recording of the emitted β pulse. At this stage the effective dead layer induced in the crystal is the dominant concern. Since this dead layer covers most of the region where the tritium is embedded the majority of β particles enter an insensitive region of the detector and are completely undetected. In fact, it was the case immediately after implanting the tritium that a β signal could not be registered in the detector.

At this stage the detector was removed from its liquid-nitrogen Dewar and allowed to warm to room temperature over a period of ~25 h. A second scan with 59-keV photons indicated that the pulse-height defect had disap-

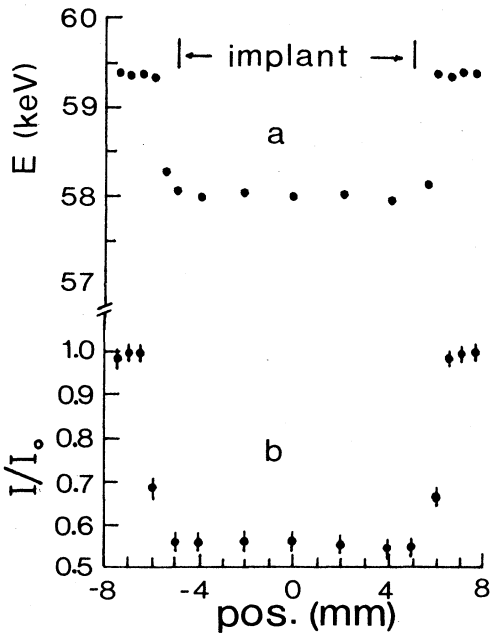

FIG. 2. Results of scanning the Ge crystal with a narrow beam of 59-keV γ rays immediately after implanting tritium. (a) A 2% pulse-height defect and (b) an ~0.59-mm dead layer were observed when photons were incident on the implanted region of the detector.

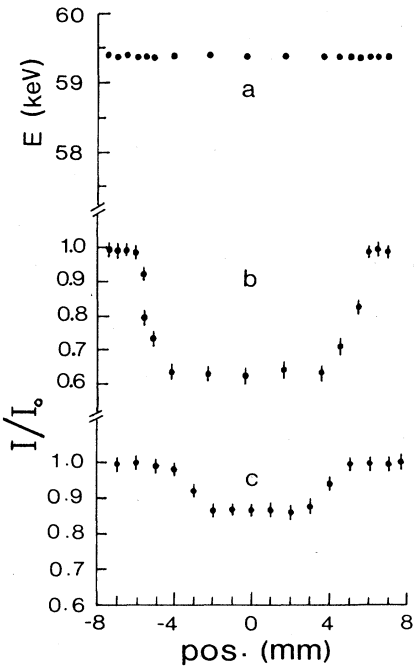

FIG. 3. Results of scanning the Ge crystal with a narrow beam of 59-keV γ rays after heating the detector. After a room temperature anneal (a) the pulse-height defect disappeared; however, (b) an ~0.45-mm dead layer remained. (c) After an *in situ* annealing phase to higher temperatures (also see Table II) the insensitive volume had dissipated both in depth and width although an ~0.14-mm dead layer remained.

peared as can be seen in Fig. 3(a). According to the result of Bourgoin *et al.*[18] simple vacancy-interstitial defects are removed from germanium with annealing temperatures just above room temperature, suggesting that the pulse-height defect was associated primarily with electron and/or hole trapping in these simple defects. However Fig. 3(b) demonstrates that an effective germanium dead layer of $\sim$0.45 mm was still present, motivating efforts to anneal the detector at higher temperatures. At this point a heavily distorted β spectrum was obtained.

Further annealing of the detector at temperatures above 25 °C was accomplished in two phases. In the first phase the germanium crystal was heated *in situ* by applying heating coils to the cold finger of the detector. It was found that an additional heating coil was required around the cryostat to achieve crystal temperatures above 90 °C. In addition, sorption pumping of the detector volume was continuously applied during the annealing procedure to take up any out-gassing from the zeolite surrounding the cold finger which could contaminate the germanium surface. A second annealing phase was carried out after removing the crystal from its cryostat.

In the first phase (*in situ* anneal) the crystal was heated in several stages to temperatures ranging from $\sim$90 to $\sim$135 °C. The duration of time for each anneal stage and the crystal temperatures maintained are listed in Table II below. At the end of each stage the detector was allowed to cool to liquid-nitrogen temperature for 24 h so that a scan of the crystal could be made using 59-keV γ rays. In this manner the effective germanium dead layer (ΔX_{Ge}) could be monitored and employed as a measure of the radiation damage remaining in the detector.

The final scan, made at the end of the *in situ* annealing phase is depicted in Fig. 3(c) where it is shown that the damaged volume of the crystal had been reduced both in depth as well as width. At this point the effective germanium dead layer was only $\sim$0.14 mm which is thin in comparison to the tritium implantation depth ($\gtrsim$0.28 mm) making it feasible to record a preliminary β spectrum. Figure 4 shows the experimental β spectrum acquired after this annealing phase. The dashed curve in this figure is a theoretical β spectrum that has been normalized to the experimental data between 1.0 and 18.6 keV. A photopeak at 11.1 keV was observed superimposed on the β spectrum. This arises from the decay of ^{73}As nuclei residual in the front of the detector that were created by $(t,2n)$ reactions during the implantation procedure. Details regarding the production of arsenic isotopes in the counter are outlined in Appendix A, and it is shown that the ^{73}As signal plays a small role when analyzing the tritium spectrum at low energies (<9 keV).

TABLE II. *In situ* annealing phase.

Crystal temperature (°C)	Duration of anneal (h)	Effective ΔX_{Ge} (mm)
1. 90	110	0.55
2. 90	135	0.51
3. 110	40	0.45
4. 110	45	0.37
5. 115	40	0.32
6. 125	65	0.24
7. 135	65	0.14

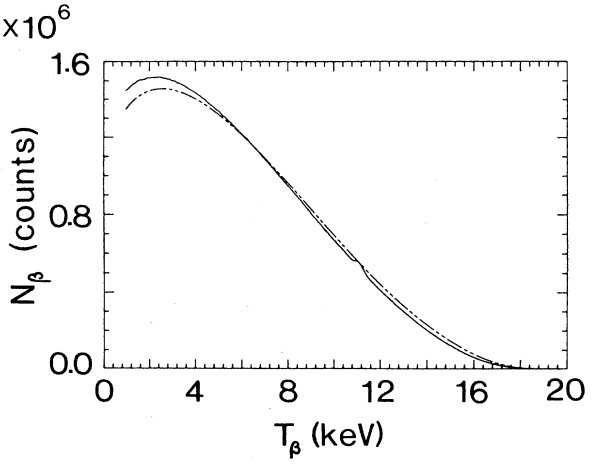

FIG. 4. Tritium β spectrum (A1) acquired after *in situ* annealing procedure. The dashed curve is a theoretical spectrum that has been normalized to the experimental area between 1.0 and 18.6 keV. The long-range curvature in the measured spectrum indicated radiation damage residual in the germanium crystal. A photopeak at 11.1 keV indicates the presence of ^{73}As isotopes in the detector.

As evident in Fig. 4 remaining radiation damage yielded long-range distortion in the measured β spectrum, indicating the need for further annealing. This was achieved by heating the germanium crystal after it was removed from its cryostat, to $\sim$180 °C for $\sim$10 h. The crystal was then reprocessed and remounted in its cryostat. Reprocessing of the crystal involved replacing the front contact of the detector which consists of a thin ($\lesssim$0.1 μm equivalent Ge), low-Z material. To do so the original contact was etched off with the result of removing an $\sim$25-μm layer of germanium from the front of the crystal. The results of this final annealing are shown in Fig. 5. In addition to a scan using 59-keV γ rays a scan was also made using the 5.9-keV x rays of ^{55}Mn. These scans serve both as a probe of the immediate detector surface and of the implanted regions. Figure 5(a) indicates no measurable pulse-height defect at 5.9 keV or at 59 keV. Figure 5(b) shows that the effective germanium dead layer has been completely removed. From the 5.9-keV x-ray scan an upper limit on the effective germanium dead layer is estimated to be $\lesssim$1.4 μm. In addition, no observable tailing effects were found in photopeaks accumulated in the implanted regions and pulse heights in implanted and nonimplanted regions agree within 0.05%. These results are consistent with expectation based on the work of Bourgoin *et al.*[18] Finally, the β count rate above 2.032 keV was the same to within 0.3% after removal of 25 μm of front surface as before, indicating that the tritium is implanted deeply into the detector as expected.

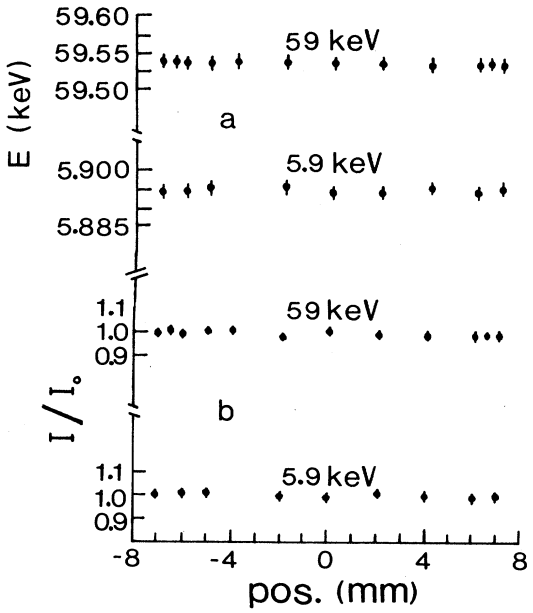

FIG. 5. Results from scanning Ge crystal with 5.9-keV x rays and 59-keV γ rays after phase II annealing. (a) Pulse heights from the implanted regions of the detector agree within 0.05% with those from the nonimplanted regions. (b) The insensitive volume of the crystal is no longer present and an estimate indicates an effective dead layer $\lesssim 1.4$ μm.

C. Calibration

Calibration of the germanium spectrometer was obtained by shining x rays on the germanium detector through its beryllium window. X-ray energies above the K-shell binding energy of germanium (11.1 keV) provide low-energy calibration lines when interactions near the surface of the crystal are accompanied by the escape of germanium K x rays. X rays with energies in the range $\sim$9.9–19.7 keV were obtained by fluorescing the appropriate materials with photons from a strong ^{109}Cd source. This source is in the shape of an annulus so that fluorescence can be observed at 180°, reducing unwanted background from both the γ ray (88.0 keV) and Ag x rays.

Table III is a list of the materials fluoresced along with the x-ray energies[23] and escape lines utilized in calibrating the spectrometer. The linearity of the spectrometer was tested by amplifying pulses from the detector preamplifier (Aptec Model SP101C) using an Ortec 572 linear amplifier. These pulses were in turn fed into an analog-to-digital converter (ADC) (Model TN-1242) and analyzed with the aid of a TN-4000 multichannel analyzer. In this configuration the spectrometer is extremely linear. The rms deviation of peak centroids from a linear calibration curve is less than $\sim$4 eV over the entire tritium energy range as is depicted in Fig. 6.

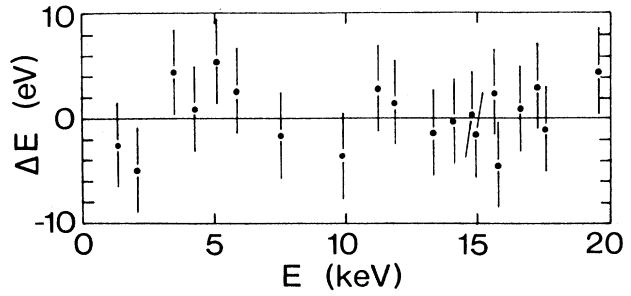

FIG. 6. Deviations of peak centroids from a linear calibration curve using the photopeaks as outlined in Table III. The rms deviation from a linear calibration is $\lesssim 4$ eV over the entire tritium energy range.

D. Spectrum recording

Beta spectra were acquired over periods of one to two weeks each before and after the final stage of annealing. In each case the detector housing was surrounded with 50 mm of lead to shield the crystal from background radiations. In addition the detector cryostat was covered successively with layers of Al (0.5 mm), Cu (1.5 mm), and Cd (2 mm) to absorb x rays produced in the outer shielding. In order to reduce background associated with low-energy acoustic noise the detector was completely housed in a soundproofing chamber.

To monitor any possible changes in calibration associated with gain and/or zero shifts, β spectra were acquired intermittently on a day-to-day basis along with the x-ray spectra obtained by fluorescing a bromine target. The centroids of these calibration lines (2.032 keV and 11.908 keV) were found to be remarkably stable and did not drift more than $\sim$3 eV over periods of one to two weeks.

Table IV outlines the β spectra accumulated after each

TABLE III. Calibration lines for hyperpure Ge spectrometer.

Material fluoresced	Element	$\bar{K}_\alpha$ (keV)	$\bar{K}_\beta$ (keV)	$\bar{K}_\alpha - \bar{K}_\alpha^{Ge}$ (keV)
Ge crystal	Ge	9.876		
Na_2SeO_4	Se	11.208		1.333
Br salt	Br	11.908		2.032
Rb salt	Rb	13.375	14.981	3.499
$SrCO_3$	Sr	14.142	15.857	4.266
Y foil	Y	14.933	16.765	5.058
Zr foil	Zr	15.746	17.699	5.870
Mo foil	Mo	17.443	19.651	7.567

TABLE IV. ^{3}H β spectra accumulated in a hyperpure Ge detector.

Spectrum	Duration (s)	Amplifier	Gain (eV/channel)	No. of channels	τ (μs)	FWHM (eV)
A1	4.89×10^5	Ortec-572	10	2048	6	405
A2	4.48×10^5	TENNELEC-242	5	2048	8	405
B	1.07×10^6	Ortec-572	5	2048	6	405
C	8.01×10^5	Ortec-572	10	2048	6	310

phase of the annealing procedure. Two β spectra were accumulated after annealing the detector *in situ* (phase I). In the first case (spectrum A1) pulses from an Ortec 572 linear amplifier were fed into an ADC (TN-1242) and recorded on a multichannel analyzer (MCA) (TN-4000) using 2048 channels for memory storage. A gain of ~10 eV/channel then allowed for data acquisition over the entire energy range of the tritium β spectrum. Data were accumulated for a period of $\sim4.9\times10^5$ s which was sufficient to achieve $\sim1.5\times10^6$ counts in 60-eV energy bins at 1.5 keV. In order to check that low-energy anomalies were not produced in the β spectrum by nonlinearities in the amplifier and/or ADC a second run was made (spectrum A2) using a TENNELEC-242 amplifier with the gain increased by a factor of 2. This spectrum is the result of data accumulation over a similar time period of $\sim4.5\times10^5$ s. There were no observable differences encountered in the linearity of the spectrometer associated with the two different amplifiers and gains used.

Two longer measurements were made after radiation-damage annealing was complete (phase II). In the first case the tritium spectrum was measured up to ~10 keV with a dispersion of ~5 eV/channel for a period of 1.07×10^6 s (spectrum B). At this stage modifications to the detector preamplifier together with a change in the detector field-effect-transistor (FET) package yielded a 25% improvement in the resolution of the spectrometer, thus motivating another measurement. Spectrum C is the result of data accumulation over a period of 8.01×10^5 s using the improved detector resolution. This measurement spanned the entire tritium energy domain up to ~20 keV using a dispersion of 10 eV/channel. The improvement in resolution for this final run is important at low energies since the signal is dominated by detector noise below ~1 keV. This point is considered in more detail in the following section.

E. Ambient background and detector noise

The tritium β signal was extracted from the raw signal after subtracting an underlying background spectrum. This background signal consists of two components: namely, ambient background related to outside radiations interacting within the germanium crystal and detector noise.

Before the tritium was implanted into the detector, an ambient background spectrum was accumulated for $\sim3\times10^6$ s over the entire tritium energy range (0–20 keV). This component of the background contributes $\sim0.01\%$ of the raw signal below ~2 keV. The ambient background signal is adequately described by a quadratic polynomial with a very small quadratic term.

At low energies ($\lesssim1$ keV) the background is dominated by detector noise. For spectrum B the resolution of the detector was ~405 eV [full width at half maximum (FWHM)] so that the tail of the low-energy noise spectrum extended up to ~1.2 keV. The shape, and intensity, of the noise signal has been studied before and after the tritium was implanted. After implanting the noise spectrum was measured with the polarity of the amplifier inverted, and in anticoincidence with noninverted pulses to reject large undershoots. It is found that the noise signal is adequately described by the tail of a Gaussian function. Figure 7 shows the characteristics at low energies from run B for the two background components described here. The total signal to β-signal ratio is given where the noise component of the background decreases rapidly from 1% of the β signal at ~0.9 keV to the ambient background level at ~1.2 keV. Also plotted in this figure is the variation in the β signal arising from a 1% branch of a 17-keV neutrino, which indicates that the noise component of the background is tolerable above ~1.2 keV.

The dashed curve in Fig. 7 is the result of a similar analysis of the background for run C where the resolution

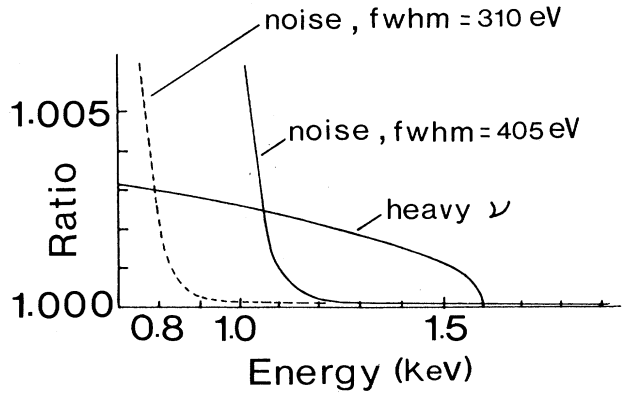

FIG. 7. The total signal to ^{3}H β-signal ratio at low energy. The solid curve indicates the ambient background plus detector noise levels relative to the tritium signal when the resolution is FWHM$\simeq$405 eV (used for spectrum B). The dashed curve represents this same function for run C with FWHM$\simeq$310 eV. Also shown is the variation in the shape of the β spectrum from a single component spectrum arising from a 1% mixing with a 17-keV neutrino.

of the detector is $\sim$310 eV. The reduction in noise for this measurement yields a low-energy tail that is negligible above $\sim$0.9 keV. As a result this spectrum gives information down to 0.9 keV that can be studied without concern for the contribution to the signal from the noise component of the background.

IV. DATA ANALYSIS

The experimental β spectra were analyzed, after background subtraction, by comparison to the theoretical shape expected from a two-state model of the electron neutrino:

$$|\nu_e\rangle = \cos\theta|\nu_1\rangle + \sin\theta|\nu_2\rangle \ . \tag{1}$$

In this case the β spectrum becomes a superposition of two single-component spectra with different end points:

$$\frac{dN(E)}{dE} = \cos^2\theta \frac{dN(E,M_1)}{dE} + \sin^2\theta \frac{dN(E,M_2)}{dE} \ , \tag{2}$$

where M_1 is the mass of the predominantly emitted light neutrino ($M_1 \approx 0$) and $\sin^2\theta$ represents the mixing probability for a heavy neutrino ($M_2 \neq M_1$). We employ the familiar single-component Fermi spectrum for the emission of a neutrino with mass M_i:

$$\frac{dN(E,M_i)}{dE} = CpEF(E,Z)(W-E)[(W-E)^2 - M_i^2c^4]^{1/2} \ . \tag{3}$$

In Eq. (3), p and E are the electron total momentum and energy, W is the total energy available to the emitted lepton field, and C is an overall normalization factor.

A modified nonrelativistic Fermi function is used in the form

$$F(E,Z) = X(1-e^{-x})^{-1}[1.002\,037 - 0.001\,427(v/c)] \ , \tag{4a}$$

where

$$X = \frac{2\pi Z\alpha}{v/c} \ . \tag{4b}$$

Here Z is the charge of the daughter nucleus, v/c is the β-particle speed relative to that of light, and α is the fine-structure constant. The linear term in Eq. (4a) is a phenomenological modification[15] to the nonrelativistic Fermi function[22] that yields the same values as the relativistic calculation of Behrens and Jänecke.[24]

While $F(E,Z)$ accommodates the Coulomb interaction between the charge on the daughter nucleus and the emitted β particle low-order corrections arise due to atomic physics. One is that the atomic electron of the daughter helium ion screens the emitted β particle from the nuclear charge. This has the effect of accelerating the β particle relative to that predicated in Eq. (4). In the classical paper by Rose,[25] the screening correction is analyzed as though the nucleus in beta decay were not aware of this screening, so that electrons are emitted into its immediate vicinity always in the same way.[5] Hence the correction is made by evaluating the electron phase-space factor and Coulomb interaction with the β energy shifted back by a constant value equivalent to the electronic potential at the origin. Use of a static potential is justified since the velocity of the β particle is high and the electron cloud distribution remains essentially unchanged during the passage of the β particle.

Several authors[3–5] have discussed the screening correction $\langle V_e \rangle$ appropriate for free atomic tritium. Lindhard and Hansen[5] have computed additional low-order corrections to the energy available to the emitted β particle by considering excited atomic final states. These include the mean excitation energy $\langle \Delta\epsilon \rangle$ released after an excited He^+ ion returns to the ground state as well as the mean neutralization energy $\langle I \rangle$ released when the daughter He^+ ion is neutralized to the ground atomic state. Since the present apparatus involves a total absorption spectrometer all of these small energy releases are accumulated in the detector. As a result the total energy registered in the detector is not available to the β particle when emitted at the nucleus and hence the statistical factor and Fermi function are computed at the experimental energies shifted by an effective screening potential $\langle V \rangle = \langle V_e \rangle + \langle \Delta\epsilon \rangle + \langle I \rangle$. While $\langle V \rangle = 65.4$ eV is the correct choice in the case of "free" atomic tritium[5] there remains some uncertainty regarding its value when tritium is bound within a crystal lattice. In particular if the effective screening potential is reevaluated for ^3H and ^3He in a uniform dielectric according to the prescription of Lindhard and Hansen,[5] its value is reduced to $\langle V \rangle = 42.6$ eV. Further discussion regarding the effective screening potential appropriate for tritium in a crystal lattice is left for Appendix B at the end of this paper, while the effect of changes to this potential on the tritium β spectrum is discussed below along with the experimental results.

V. RESULTS

Radiation damage residual in the detector after the *in situ* annealing phase yielded long-range distortion in the measured β spectra (A1 and A2) making a comparison with a theoretical spectrum difficult. However, since the signature for heavy neutrino emission is a sudden distortion it was feasible to explore these spectra over narrow energy intervals in search of anomalies associated with a threshold phenomenon. Apart from resolution effects, it is straightforward to show that the deviation ΔK in the Kurie plot K with nonzero M_2 from that with $\sin\theta = 0$ is given by

$$\frac{\Delta K}{K} \simeq \frac{\tan^2\theta}{2}\left[1 - \frac{M_2^2c^4}{(Q-E_\beta)^2}\right]^{1/2} \ , \tag{5}$$

where the deviation is nonzero for $Q - E_\beta > M_2c^2$.

Figure 8 shows the fractional deviations $\Delta K/K$ obtained from the measured β spectra A1 and A2 accumulated after phase I of the annealing procedure. Kurie plots were calculated from the measured β intensity using the Fermi function described in Eq. (4) and an effective screening potential of 42.6 eV. In this preliminary analysis a straight line was fit to the Kurie plots between $\sim$2 and 3 keV. The deviation from this linear fit below 2

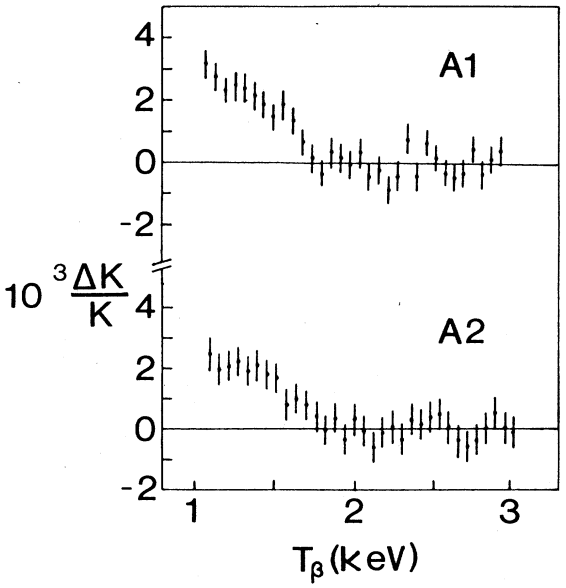

FIG. 8. Deviations $\Delta K/K$ below ~ 2 keV in the Kurie plots of spectrum A1 and A2 from a linear Kurie plot obtained by fitting a straight line to the Kurie plot K between 2 and 3 keV.

keV then represents the deviation between the experimentally determined Kurie plot and that expected from the emission of a single-component, light neutrino. To check whether or not this nonzero anomaly is a result of radiation damage residual in the counter a similar exercise was performed for 2-keV windows up to ~ 10 keV . Figure 9 shows the results of this analysis, where the deviations $\Delta K/K$ obtained from spectrum A1 are plotted. As indicated in this figure there is no sign of a sudden distortion in the Kurie plot above 2 keV. An independent analysis of spectrum A2 in this way yields similar conclusions. Furthermore, the distortion below 2 keV is found at the same pulse height in both spectra A1 and A2 suggesting that the observed anomaly does not arise from nonlinearities in the amplifier or ADC.

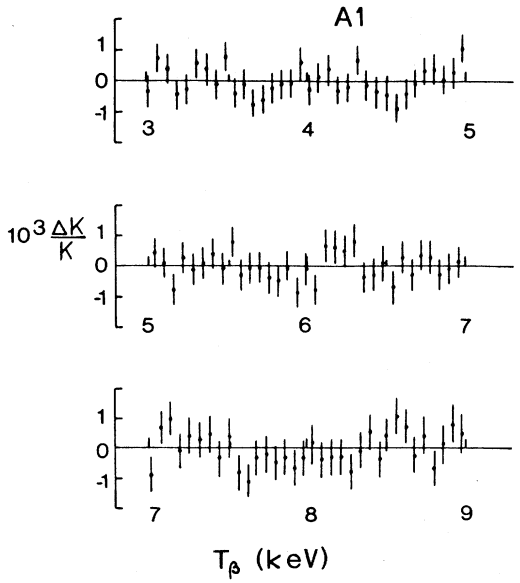

FIG. 9. Deviations $\Delta K/K$ in the Kurie plot of spectrum A1 obtained by fitting the experimental Kurie plot to a straight line over 2-keV energy windows. There is no sudden distortion as is the case between 1 and 3 keV. A similar analysis using the Kurie plot obtained from spectrum A2 yields the same results.

The β spectra accumulated after annealing was complete (runs B and C) were examined more thoroughly by direct comparison to a theoretical spectrum as prescribed by Eq. (2). Comparison was made by computing a theoretical spectrum convoluted with the experimental resolution function at the experimental energies. In this case the experimental response is treated as Gaussian with FWHM determined from x-ray spectra and a precision pulser. The resolution used for spectrum B and spectrum C were 405 eV and 310 eV, respectively.

The experimental spectra were first analyzed by comparison to a theoretical spectrum without a heavy neutrino mixed in ($\sin^2\theta=0$) by allowing the end-point energy to vary together with an overall normalization constant while fitting. Results of this fitting procedure are shown in Fig. 10 where the shape factors are plotted for spectra B and C. These shape factors were obtained by taking the ratio of the experimental β spectra to the best theoretical least-squares fit with $\sin^2\theta=0$ using an effective screening potential of 42.6 eV. The experimental shape is consistent with unity apart from a sudden ex-

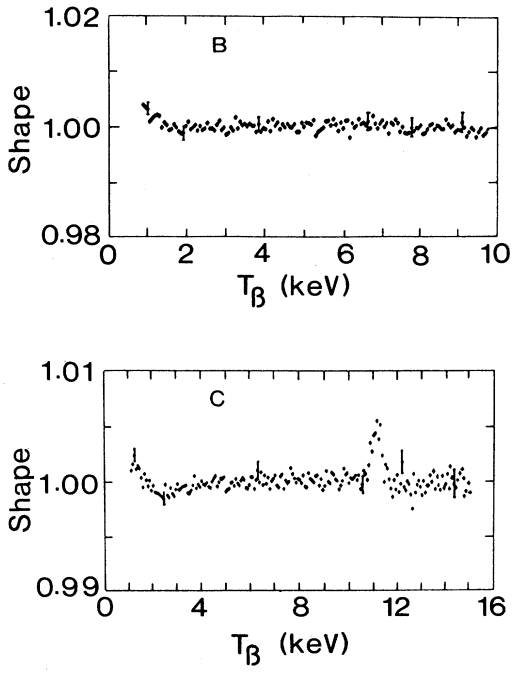

FIG. 10. Shape factors obtained by taking the ratio of the measured β-spectra B and C to the best least-squares fit to a single-component Fermi spectrum using an effective screening potential of 42.6 eV. The peak at 11 keV in C is due to ^{73}As decay. There is a sudden excess of counts below ~ 2 keV in both runs B and C.

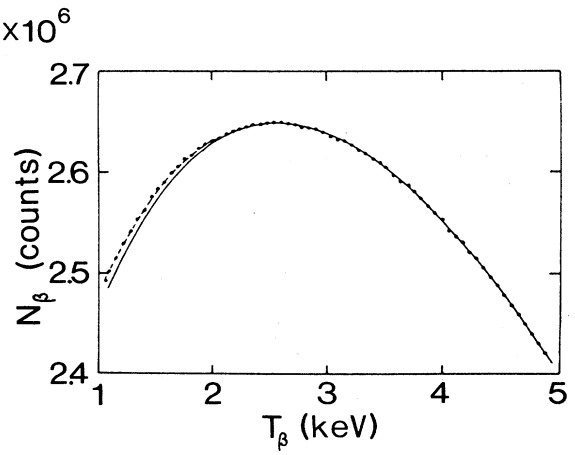

FIG. 11. Low-energy portion of the tritium β spectrum of run B obtained after background subtraction. The smooth curve is a single-component Fermi spectrum that has been fit to the experimental points between 2.5 and 6.0 keV.

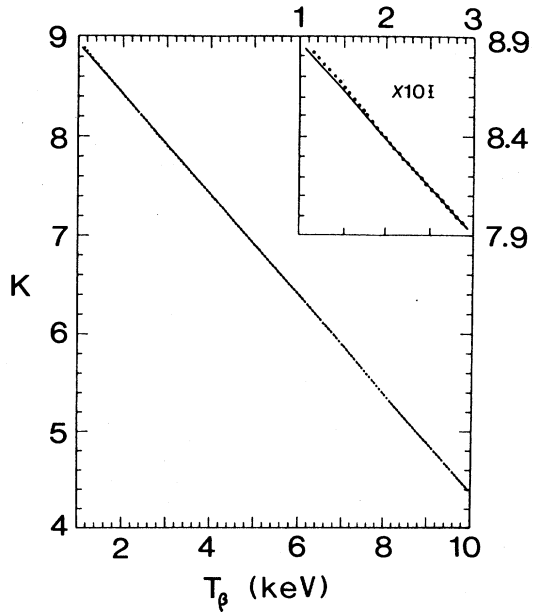

FIG. 12. Kurie Plot obtained from the β intensity of run B using an effective screening potential of 42.6 eV. The expanded version in the upper right indicates the excess of counts observed in the spectrum below $T_\beta \simeq 2$ keV (the error bar shown is ten times larger than the true error bar).

cess of counts below ~ 2 keV. The shape factor for spectrum C includes a photopeak at 11.1 keV (equivalent to the K-shell binding energy of Ge) and is indicative of ^{73}As decaying in the detector. The amount of $L1$ capture of ^{73}As has been estimated from the K-capture peak to contribute about 4% to the excess counts due to the heavy neutrino in run C, and the contribution from K capture followed by escape of the K_α x ray much less than 3%. (See Appendix A.)

Figure 11 shows a portion of β spectrum B between 1 and 5 keV. The smooth curve through the experimental points is a single-component Fermi spectrum that has been fit to the data between 2.5 and 6.0 keV. The end-point value obtained in fitting this region was 18.62±0.01 keV which is in reasonable agreement with the accepted value for tritium of 18.60 keV (Ref. 26), considering that the fitting is done far from the end point. When the smooth curve is extrapolated to 1 keV the experimental points deviate from this single-component spectrum below 2 keV. The corresponding Kurie plot has been obtained from this β spectrum using an effective screening potential of 42.6 eV and is shown in Fig. 12. To emphasize the excess of counts observed in the low-energy region of the tritium spectrum an expanded region of the Kurie plot between 1.0 and 3.0 keV is given in the upper right of this figure where the deviation from a straight line below ~ 2 keV is clearly evident.

The tritium spectra from runs B and C were compared to a two-state model of the electron neutrino by allowing the end-point energy, mixing probability, and the threshold energy $E_{\rm th}$ for the emission of a heavy neutrino all to vary along with an overall normalization constant. The data were analyzed from 1.2 keV for run B and from 0.9 keV for run C up to a β-kinetic energy of ~ 3.2 keV employing an effective screening potential of 42.6 eV. The results of fitting are outlined in Fig. 13 and Table V where the absolute minimum in χ^2 is plotted for a given value of R ($=\sin^2\theta$) after allowing all other parameters to

TABLE V. Results from fitting ^{3}H spectra.

Run	$\langle V \rangle$ (eV)	$Q_{\rm fit}$ (keV)	$E_{\rm th}$ (keV)	$\sin^2\theta$ (%)[a]	M_2 (keV)[b]	χ^2/ν
B	42.6	18.616	1.75±0.10	0.90±0.20	16.85±0.10	35.8/32
C		18.678	1.60±0.10	1.32±0.20	17.00±0.10	28.5/32
Combined				1.11±0.14	16.93±0.07	
B	65.4	18.512	1.72±0.10	1.15±0.20	16.88±0.10	36.9/32
C		18.617	1.58±0.10	1.74±0.20	17.02±0.10	29.3/32
Combined				1.45±0.14	16.95±0.07	

[a]Correction for L capture of ^{73}As has not been included (see text).
[b]Assuming an end-point energy of 18.6 keV.

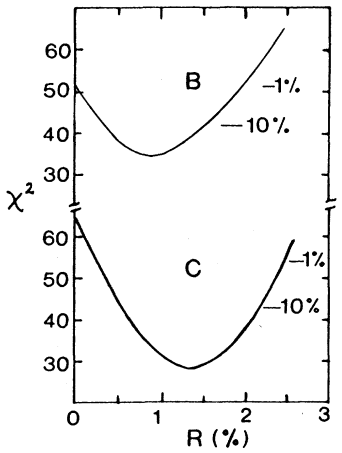

FIG. 13. χ^2 plots obtained by fitting spectrum B and spectrum C to a two-state model of the electron neutrino using an effective screening potential of 42.6 eV. A combined χ^2 indicates that the data are best described by the emission of 16.93±0.10 keV neutrino with a (1.1±0.2)% mixing probability.

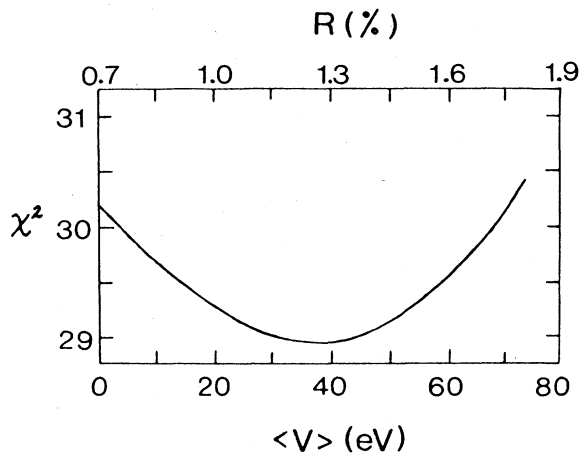

FIG. 15. χ^2 plot obtained by fitting spectrum C with the effective screening potential $\langle V \rangle$ as a free parameter. An absolute minimum is obtained with $\langle V \rangle = 38 \pm 20$ eV; however χ^2 is not a strong function of this parameter. Also shown are the values of $R = \sin^2\theta$ at which χ^2 is an absolute minimum for a given $\langle V \rangle$.

vary. The data seem to be best described by a two-state spectrum involving the emission of a 16.93±0.07 keV neutrino and a mixing probability of (1.1±0.2)%. When we allow for contribution to the kink from L-capture decay of ^{73}As in runs B and C the central value of the mixing probability reduces to (1.0±0.2)%. (See Appendix A.) Figure 14 shows the deviations ΔK from a linear Kurie plot K for spectra B and C, respectively. The smooth curves through the experimental points are predicted as in Eq. (5) for the emission of a heavy neutrino after accounting for resolution smearing.

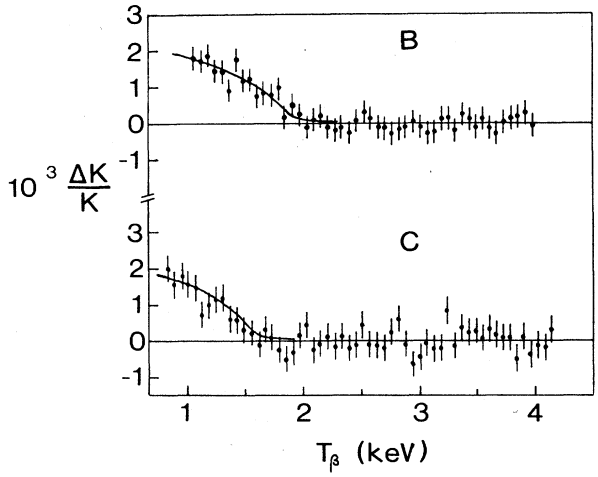

FIG. 14. The fractional deviations $\Delta K/K$ in the Kurie plots of spectrum B and spectrum C from a straight line using an effective screening potential of 42.6 eV. The smooth curves are as predicted in Eq. (5) for the emission of a heavy neutrino after accounting for resolution smearing. $M_2 = 16.85$ keV with $\sin^2\theta = 1.1\%$ in the case of spectrum B with FWHM $\simeq$ 405 eV. $M_2 = 17.00$ with $\sin^2\theta = 1.3\%$ in the case of spectrum C with FWHM = 310 eV.

In order to demonstrate the effect of altering the effective screening potential in the case of atomic tritium a separate analysis has been performed using an effective screening potential of 65.4 eV which is considered to be the correct choice for free tritium. The effect of increasing the screening potential is to increase the deduced value for the mixing probability to (1.5±0.2)%. The χ^2 plot in Fig. 15 is the result of fitting β spectrum C to a two-state model for various values of the effective screening potential ranging between 0 and 80 eV. Although an absolute minimum occurs at ~40 eV the goodness of fit is not a strong function of the screening potential used. However it is important to emphasize that even when zero screening is used the excess of counts at low energy is not completely removed. Changes to the effective screening potential only shift the deduced mixing probability for a 17-keV neutrino. Values for a heavy neutrino branch range from 0.6 to ~1.9% when scanning the effective screening potential between 0 and 80 eV; however, even when $\langle V \rangle$ is set to zero, $\sin^2\theta = 0$ is still ruled out at the 92% confidence level when the results of runs B and C are combined.

These results are in good agreement with those obtained by measuring the β spectrum of tritium implanted into a Si(Li) detector as outlined in Appendix C of this paper.

VI. DISCUSSION

We now have the results from two independent measurements on the β spectrum of tritium, each showing a marked distortion 17 keV below the end point. Furthermore the amplitude of the observed distortion is the same whether using a germanium or a Si(Li) detector. While a similar technique has been employed to measure the tritium spectrum using two different types of semiconductor

detectors the distortion observed seems to be independent of solid-state effects or small amounts of radiation damage. These conclusions are strengthened upon considering the following points.

(i) While it is generally difficult to calibrate Si detectors below ~ 5 keV, calibration of the germanium spectrometer has been achieved as low as 1.3 keV with the use of escape x rays. Consequently, the observed distortion cannot be attributed to uncertainties in the detector response at low energies.

(ii) Analysis of tritium spectra (A1 and A2) accumulated after *in situ* annealing indicate that the effect of residual radiation damage in the detector is to introduce long-range curvature into the β spectrum. However, a sudden distortion was observed in these spectra below ~ 2 keV. Further annealing of the germanium crystal to higher temperatures removed all remaining observable radiation damage in the detector, but, the sudden excess of counts below ~ 2 keV was still observed (spectra B and C) after this stage of the anneal cycle. Furthermore, the distortion occurs at the same threshold energy and with the same magnitude after each stage of the anneal cycle, indicating that the threshold distortion noted is inherent in the β signal.

(iii) Finally, the possibility of systematic uncertainties in the low-energy region of the tritium spectrum arising from nonlinearities in the amplifier and/or ADC has been negated by performing separate measurements with different amplifiers and different amplifier gains. The fact that the distortion observed always occurs at the same energy with the same amplitude and shape indicates that the effect is inherent in the signal and not in the associated electronics processing the signal.

To summarize, the agreement between results from independent experiments using Si(Li) and Ge detectors leads to the conclusion that the distortion observed is manifest in the physics governing the tritium β decay. While the data are best described with the emission of a 17-keV neutrino with $\sin^2\theta=(1.0\pm0.2)\%$, the value of the mixing probability is dependent on the state of ^{3}H and ^{3}He in a crystal lattice. However, if we consider a range of values for the effective screening potential between zero and the value for free tritium of 65.4 eV we obtain the range $0.6 \leq \sin^2\theta \leq 1.6\%$ for the mixing probability associated with a 17-keV component to the electron neutrino. Unfortunately, χ^2 is not a strong function of this potential so that its value is not uniquely determined by fitting. In any case it would seem that $\sin^2\theta=0$ is completely ruled out. The interpretation of the distortion as due to a heavy neutrino is also strengthened by the ^{35}S data reported in the preceding paper.[14]

VII. CONCLUSION

If the present interpretation of the ^{3}H and ^{35}S β spectra is correct, these results provide evidence that neutrinos have mass and that mixing takes place between different neutrino generations. This immediately introduces the possibility of neutrino oscillations. At present the best limits on small mixing angles are from "appearance" experiments at accelerators, where the nonobservation of $\nu_e \leftrightarrow \nu_\mu$ and $\nu_e \leftrightarrow \nu_\tau$ oscillations gives the following upper bounds on $\sin^2\theta$ for large neutrino mass differences:[27]

$$\sin^2\theta_{e\mu} < 0.001, \quad \sin^2\theta_{e\tau} < 0.04 .$$

Consequently, the nonobservation of $\nu_e \leftrightarrow \nu_\mu$ oscillations at the present limit suggests that the 17-keV neutrino reported here cannot be the dominant component of the muon neutrino. If it is the dominant component of the tau neutrino then an increase in sensitivity to the $\nu_e \leftrightarrow \nu_\tau$ channel of about a factor of 5 could yield observation of neutrino oscillations in the future. Furthermore, if the dominant mass component of the muon and tau neutrinos is 17 keV or less it will be difficult to measure these masses directly by conventional techniques.

A 17-keV neutrino that represents a $\sim 1\%$ component of the electron neutrino would contribute an effective mass,[28] $M_2\sin^2\theta$, for neutrinoless 2β decay of ~ 170 eV. This contribution is much larger than inferred from present experimental limits for this process,[29] suggesting that neutrinos are Dirac particles. An alternative explanation,[30] would seem to require that the dominant component of the muon neutrino have a mass greater than ~ 68 keV.

Cosmological constraints on massive neutrinos[31] would suggest that a 17-keV neutrino would have to be unstable and decay with a mean life $\lesssim 7\times10^{11}$ sec. If we adhere to the constraints imposed on massive neutrinos by the standard "hot big bang" model it then becomes a problem of particle physics to provide the mechanism by which a 17-keV neutrino could decay. Studies of decay modes for heavy neutrinos using various extensions of the standard model have been carried out[32] for the three known generations of leptons. In all cases explored the lifetime predicted for a 17-keV neutrino is too long to satisfy the cosmological constraints, which suggests that there exists new particle physics beyond the standard model, unless there is something inherently lacking in our understanding of cosmology. It is interesting to point out that Holdom[33] has taken the technicolor approach whereby a 17-keV neutrino can decay via a techniphoton with a half-life that falls well within the constraints of cosmology. This possibility is interesting since the model involves an $L_e-L_\mu+L_\tau-L_\lambda$ symmetry, where λ represents a fourth-generation lepton, and can accommodate the nonobservation of $\nu_e \leftrightarrow \nu_\mu$ oscillations.

ACKNOWLEDGMENTS

The authors are grateful to the accelerator crew at McMaster University for their help with the tritium beam, as well to W. R. Dixon of NRC (Canada) for the use of the germanium detector, J. L. Campbell of the University of Guelph for the use of his x-ray scanning instrument, and Doug Brooks at Aptec Engineering for his continuous efforts in maintaining and improving the performance of the detector. We also acknowledge the financial support of the Natural Sciences and Engineering Research Council, Canada for A.H.

APPENDIX A: ARSENIC ISOTOPES

Nuclear transmutations of germanium can be induced when the incident triton energy is large enough to overcome the Coulomb potential (~ 7.9 MeV) between the

tritium and germanium nuclei. After implanting the detector an energy spectrum up to ~ 1 MeV was acquired which indicated the presence of unstable arsenic isotopes produced by (t,n) and $(t,2n)$ reactions within the sensitive volume of the detector. At the triton energies used for implantation an estimate shows that these isotopes can be produced at depths up to ~ 0.15 mm. Table VI lists those reactions that yield the observed arsenic isotopes together with an estimate of their respective Q values. Decay modes for each isotope, together with their respective half-lives are also included.[22] Only one of the isotopes produced (^{75}As) is stable. All other decay modes yield stable isotopes of germanium, selenium, and gallium. Studies[34] on the presence of As, Se, and Ga impurities in germanium show that these sites can serve as donor or acceptor levels to photoelectrons produced in the crystal by ionizing radiations. However, at liquid-nitrogen temperatures these are neutral sites and thus do not affect the electrical properties of the semiconductor.[35]

The time between implanting the tritium and the end of radiation damage annealing was about one year so that all short-lived isotopes are no longer observable. Furthermore, removal of a 25-μm layer of germanium from the front of the detector reduces the number of arsenic decays since isotopes produced near the surface of the detector were removed. The only remaining concern when measuring the tritium β spectrum is background radiations produced by the longer-lived ^{73}As ($T_{1/2} \sim 80$ days) isotope.

^{73}As decays primarily by K-electron capture to the 66.7-keV state of ^{73}Ge. The K shell is filled in a short time ($\sim 10^{-16}$ s) relative to the lifetime of the excited nuclear state (0.5 s) so that each decay is accompanied by a pulse at ~ 11.1 keV corresponding to the K-shell binding energy of a germanium atom. Since we are interested in a region of the β spectrum in the neighborhood of 1.0–5.0 keV this does not pose as a hazard for analyzing the tritium spectrum. However, the 53-keV γ rays associated with the deexcitation of the germanium nucleus may provide a background at low energies if they Compton scatter out of the germanium crystal. An estimate has been made of the rates of ^{73}As decay within the detector volume by measuring the rate of 11.1-keV pulses. Since the arsenic isotopes exist only near ($\lesssim 0.15$ mm) the front surface of the detector the efficiency for absorbing the γ rays emitted toward the front of the crystal is greatly reduced. However, the decay of these excited states is predominately via the emission of conversion electrons ($e_K/\gamma = 7.2$ for the 53-keV level) as opposed to photons. An estimation of the upper limit to the background produced in the region 1–3 keV from photons that Compton scatter out of the detector yields a rate $\lesssim 2\times 10^{-7}$ relative to the strength of the β signal in this energy region which is completely negligible.

K capture might also be followed by the escape of a K_α x ray leading to a peak near 1.23 keV. In a measurement similar to those made for energy calibration (see Sec. III C) the K-escape peak has an intensity of 6.8% of the Ag K_α peak itself. The K x rays of Ag have about the same absorption length as the Ge K_α x ray itself in germanium. Since 88% of the K x rays of Ag interact by producing a K vacancy,[36] the K escape per K vacancy produced is about 7.7%. Using the K-capture peak at 11.1 keV in run C and K-escape probability of 7.7% leads to an excess of 1800 counts around 1.23 keV, which is about 3% of the excess counts observed in the low-energy region. However, the ^{73}As is estimated to be distributed to greater depths, ~ 150 μm, than the absorption length of the Ge K_α x rays in germanium, about 70 μm. If in addition we assume a uniform distribution for ^{73}As, which is more likely than the exponential distribution of the Ag x rays, then the K-escape fraction will be much smaller and we have not corrected for it.

The second important decay mode of ^{73}Ag is by $L1$ capture which produces a peak at 1.41 keV. This can be estimated from the K-capture peak at 11.1 keV using the EC($L1$)/EC(K) ratio of 0.1[23] to contribute about 2300 counts to the β spectrum of run C around 1.4 keV, which is about 4.3% of the excess counts observed in the low-energy region.

Finally, these estimates can be shown to be reasonable because runs A1, A2, B, and C were well spread out in time. Runs A1, A2, and B were made 3.8, 3.6, and 1.6 half-lives of ^{73}As before run C, but there are no large time variations evident in the data. (See Figs. 8 and 14.)

TABLE VI. Production of As isotopes in a hyperpure Ge detector.

Estimated Q value (MeV)	Reaction	Decay mode	$T_{1/2}$
−3.86	^{70}Ge$(t,2n)^{71}$As	$\rightarrow {}^{71}$Ge$\rightarrow {}^{71}$Ga	12 d
+4.55	^{70}Ge$(t,n)^{72}$As	$\rightarrow {}^{72}$Ge	26 h
−2.83	^{72}Ge$(t,2n)^{73}$As	$\rightarrow {}^{73}$Ge	80 d
+5.16	^{72}Ge$(t,n)^{74}$As	$\rightarrow {}^{74}$Ge, ^{74}Ga	18 d
−1.63	^{73}Ge$(t,2n)^{74}$As		
+8.62	^{73}Ge$(t,2n)^{75}$As	Stable	
−1.58	^{74}Ge$(t,2n)^{75}$As		
+5.75	^{74}Ge$(t,n)^{76}$As	$\rightarrow {}^{76}$Se	26 h
−0.49	^{76}Ge$(t,2n)^{77}$As	$\rightarrow {}^{77}$Se	39 h
+6.41	^{76}Ge$(t,n)^{78}$As	$\rightarrow {}^{78}$Se	91 min

APPENDIX B: SCREENING CORRECTIONS

Lindhard and Hansen[5] have discussed the effective screening potential required for correcting the Fermi function in the case of the β decay of atomic tritium in a calorimetric type of measurement. This includes a screening correction $\langle V_e \rangle$, a mean excitation energy $\langle \Delta\epsilon \rangle$ released when an excited He^+ ion returns to the ground state, and a mean neutralization energy $\langle I \rangle$ released when the daughter He^+ ion is neutralized to the ground atomic state. The sum of these three contributions yields an effective screening potential $\langle V \rangle$ which takes the value 65.4 eV in the case of "free" atomic tritium. However, studies[37,38] of muonium in germanium and silicon lattices find that the electron probability at the muon is reduced significantly in comparison to that of muonium in vacuum:

$$|\psi(0)|^2_{Ge}=0.58|\psi(0)|^2_{vac} ,$$

$$|\psi(0)|^2_{Si}=0.44|\psi(0)|^2_{vac} .$$

If this reduction is to be attributed to muonium in a uniform dielectric[39] one estimates a dielectric constant of ~ 1.2 for germanium and ~ 1.3 for silicon. Since it is believed[40] that hydrogen in germanium behaves similarly to muonium in germanium it is reasonable to expect that the probability for the atomic electron to be at the nucleus is similarly affected. If we make the assumption that the effect of the dielectric is the same for both tritium and helium in a lattice the effective screening potential can be shown to be inversely proportional to the square of the dielectric constant and is ~ 43 eV for ^3H in Ge and ~ 38 eV for ^3H in Si.

APPENDIX C: TRITIUM IN A Si(Li) DETECTOR

In light of our discussion concerning the appropriate choice of the effective screening correction when tritium is bound within a lattice and the effect this choice has on the branching fraction for a 17-keV neutrino the earlier data of the β spectrum of ^3H in a Si(Li) detector has been reexamined by allowing $\langle V \rangle$ to vary as a free parameter. The results of fitting the three tritium spectra of Ref. 1 between 0.7 and 3.5 keV are shown in Fig. 16 for $\langle V \rangle$ between 0 and 65 eV. Also shown are the values of $\sin^2\theta$ where χ^2 minimizes for a particular choice of the effective screening potential. Values of the mixing probability for a 17-keV neutrino range from 0.5 to 1.8% with an absolute minimum occurring at $\langle V \rangle = 38 \pm 10$ eV and $\sin^2\theta = (1.1 \pm 0.3)\%$. These results are in complete agreement with those obtained from measuring the tritium β spectrum in germanium.

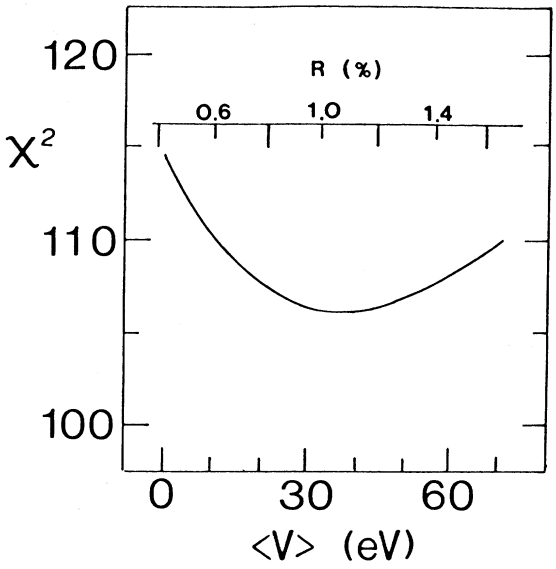

FIG. 16. Results from fitting the three spectra of Ref. 1 for tritium in Si(Li) to a two-state model of the electron neutrino while allowing the effective screening potential to vary as a free parameter. A minimum in χ^2 occurs for 102 degrees of freedom at $\langle V \rangle = 38 \pm 10$ eV and $\sin^2\theta = (1.1 \pm 0.3)\%$ for a 17-keV neutrino. The upper abscissa gives the values of $R = \sin^2\theta$ at which χ^2 is an absolute minimum for a given $\langle V \rangle$.

*Present address: Department of Nuclear Physics, University of Oxford, Nuclear Physics Laboratory, Keble Road, Oxford, England OX1 3RH.

[1]J. J. Simpson, Phys. Rev. Lett. **54**, 1891 (1985).
[2]J. J. Simpson, in *Massive Neutrinos in Particle Physics and Astrophysics,* proceedings of the Twenty-First Rencontre de Moriond (VIth Workshop), Tignes, France, 1986, edited by O. Fackler and J. Tran Thanh Van (Editions Frontières, Gif-sur-Yvette, 1986), p. 565.
[3]B. Eman and D. Tadić, Phys. Rev. C **33**, 2128 (1986).
[4]E. G. Drukarev and M. I. Strikman, Zh. Eksp. Teor. Fiz. **91**, 1160 (1986) [Sov. Phys. JETP **64**, 686 (1986)].
[5]J. Lindhard and P. G. Hansen, Phys. Rev. Lett. **57**, 965 (1986).
[6]W. Haxton, Phys. Rev. Lett. **55**, 807 (1985).
[7]T. Altzitzoglou, F. Calaprice, M. Dewey, M. Lowry, L. Piilonen, J. Brorson, S. Hagen, and F. Loeser, Phys. Rev. Lett. **55**, 799 (1985).
[8]V. M. Datar, C. V. K. Baba, S. K. Bhattacherjee, C. R. Bhuinya, and A. Roy, Nature (London) **318**, 547 (1985).
[9]A. Apalikov, S. D. Boris, A. I. Golutvin, L. P. Laptin, V. A. Lyubimov, N. F. Myasoedov, U. V. Nagovitsyn, E. G. Novikov, V. Z. Nozik, V. A. Suloshchenku, I. N. Tikhomirov, and E. F. Tret'yakov, Pis'ma Zh. Eksp. Teor. Fiz. **42**, 233 (1985) [JETP Lett. **42**, 289 (1985)].
[10]T. Ohi, M. Nakajima, H. Tamura, T. Matsuzaki, T. Yamazaki, O. Hashimoto, and R. S. Hayano, Phys. Lett. **160B**, 322 (1985).
[11]J. Markey and F. Boehm, Phys. Rev. C **32**, 2215 (1985).
[12]J. J. Simpson, Phys. Lett. B **174**, 113 (1986).
[13]D. W. Hetherington, R. L. Graham, M. A. Lone, J. S. Geiger, and G. E. Lee-Whiting, Phys. Rev. C **36**, 1504 (1987).
[14]J. J. Simpson and A. Hime, preceding paper, Phys. Rev. D **39**, 1829 (1989).
[15]J. J. Simpson, Phys. Rev. D **23**, 649 (1981).

[16]G. Dearnaley and D. C. Northrup, in *Semiconductor Counters for Nuclear Radiations,* 2nd ed. (Wiley, New York, 1966).
[17]W. R. Dixon, R. S. Storey, and W. F. Davidson, Nucl. Instrum. Methods **B12**, 304 (1985).
[18]J. C. Bourgoin, P. M. Mooney, and F. Poulin, in *Defects and Radiation Effects in Semiconductors,* 1981, edited by R. R. Hariguti (Institute of Physics Conference Series No. 59) (IOP, Bristol, 1981), p. 33.
[19]W. L. Hansen, E. E. Haller, and P. Luke, IEEE Trans. Nucl. Sci. **NS-29**, No. 738 (1982).
[20]H. F. Schopper, in *Weak Interactions and Nuclear Beta Decay* (North-Holland, Amsterdam, 1966).
[21]C. F. Williamson, J. Boujot, and J. Picard, in *Tables of Range and Stopping Power of Chemical Elements for Charged Particles of Energy 0.5 to 500 MeV* (Centre D'Etudes Nucleaires de Saclay Report CEA-R 3042, Saclay, France, 1966).
[22]P. Marmier and E. Sheldon, *Physics of Nuclei and Particles,* VI (Academic, New York, 1969), p. 360.
[23]*Table of Isotopes,* 7th ed., edited by G. M. Lederer and V. S. Shirley (Wiley, New York, 1978).
[24]H. Behrens and J. Jänecke, *Landolt-Bornstein, New Series* (Springer, Berlin, 1969), Group I, Vol. 4.
[25]M. E. Rose, Phys. Rev. **49**, 727 (1936).
[26]G. Audi, R. L. Graham, and J. S. Geiger, Z. Phys. A **321**, 533 (1985); J. J. Simpson, W. R. Dixon, and R. S. Storey, Phys. Rev. C **31**, 1891 (1985).
[27]F. Vannucci (unpublished).
[28]J. J. Simpson, Phys. Lett. **102B**, 36 (1981).
[29]D. O. Caldwell, Nucl. Instrum. Methods **A264**, 106 (1988).
[30]M. J. Dugan, A. Manohur, and A. E. Nelson, Phys. Rev. Lett. **55**, 170 (1985).
[31]D. A. Dicus, E. W. Kolb, and V. L. Teplitz, Phys. Rev. Lett. **39**, 168 (1977).
[32]H. Harari and Y. Nir, Nucl. Phys. **B292**, 251 (1987).
[33]B. Holdom, Phys. Lett. **160B**, 303 (1985).
[34]S. M. Sze, *Physics of Semiconductor Devices* (Wiley, New York, 1969), p. 20.
[35]C. Fisher, private communication.
[36]J. H. Scofield, Report No. UCRL-51326, 1973 (unpublished).
[37]J. H. Brewer *et al.*, Phys. Rev. Lett. **31**, 143 (1973).
[38]I. I. Gurevich *et al.*, Zh. Eksp. Teor. Fiz. **60**, 471 (1971) [Sov. Phys. JETP **33**, 253 (1970)].
[39]J. S. Y. Wang and C. Kittel, Phys. Rev. B **7**, 713 (1973).
[40]Bruce D. Patterson, Rev. Mod. Phys. **60**, 69 (1988).